Available online at www.sciencedirect.com
ScienceDirect
Solid State Communications 139 (2006) 581–588
solid state communications
www.elsevier.com/locate/ssc

Mechanisms of the giant electrorheological effect

Xianxiang Huang[a], Weijia Wen[a], Shihe Yang[b], Ping Sheng[a,*]

[a] *Department of Physics and Institute of Nano Science and Technology, The Hong Kong University of Science and Technology, Clear Water Bay, Kowloon, Hong Kong, China*
[b] *Department of Chemistry and Institute of Nano Science and Technology, Hong Kong University of Science and Technology, Clear Water Bay, Kowloon, Hong Kong, China*

Received 10 April 2006; accepted 11 April 2006 by P. Sheng

Abstract

Electrorheology (ER) denotes the control of rheological characteristics through applied electric field. ER fluids constitute a class of colloids whose viscosity can increase under increasing electric field. Under very strong fields some ER fluids can turn into anisotropic solids, characterized by a yield stress. The recent discovery of the giant electrorheological (GER) effect in suspensions of nanoparticles has challenged the conventional wisdom on ER fluids, as the GER fluids can break the theoretical upper bound on the (high-field state) yield stress. Starting from experimental observations of the GER characteristics, we show that the model of aligned molecular dipole layers in the contact region of coated nanoparticles can yield predictions in excellent agreement with measured data. The statistical mechanics of the aligned dipole layers is studied through Monte Carlo simulations. We propose electrowetting between the particles and the suspending liquid, with hydrogen bonding as a contributing element, in inducing the aligned state.

PACS: 83.80.Gv; 82.70.-y; 41.20.-q

Keywords: A. Colloids; D. Electrorheology; D. Molecular dipoles; D. Coated nanoparticles

1. Introduction

Electrorheological fluids [1–13] constitute a type of colloidal suspensions consisting of dielectric particles dispersed in an insulating oil. The marvelous feature of an ER fluid is that it can solidify into a jelly-like state almost instantaneously (1–10 ms) when subject to an externally applied electric field with moderate strength (a few kV/mm), with a stiffness varying proportionally to the field strength. The liquid–solid transformation is reversible. Once the applied field is removed, the original flow state is recovered. Such characteristics enable ER fluids to be an electro-mechanical interface that, when coupled with motion sensors and electronic control systems so as to correlate external conditions with the ER characteristics, can mean controllability and responsiveness of mechanical devices. In particular, ER-based active dampers and clutches have recently been demonstrated [14–17]. However, ER fluids have yet to find widespread commercial applications, mainly due to the fact that the maximum yield stress achievable by most of the conventional ER fluids is less than 10 kPa, much below ∼30 kPa required by many mechanical devices.

Recently, a new type of ER fluid with the giant electrorheological (GER) effect was discovered [18]. The GER fluids consist of coated nanoparticles ($BaTiO(C_2O_4)_2 + NH_2CONH_2$) suspended in silicone oil. In the core/shell structure (Fig. 1(a)), the urea coating serves as an ER promoter. Under an applied electric field, induced polarization in the particles causes their aggregation into columns aligned along the field direction (Fig. 1(b)). These columns are responsible for the solid-like yield stress when sheared perpendicular to the columns. A closer look at one of the columns is shown in Fig. 1(c), where it is seen that the particles' contact areas are somewhat flattened, indicating a degree of softness in the coatings.

The static yield stress curves for two volume fractions, measured under DC electric fields, are shown in Fig. 2. For

---

[*] Corresponding author. Fax: +852 2358 1652.
E-mail address: sheng@ust.hk (P. Sheng).

0038-1098/$ - see front matter
doi:10.1016/j.ssc.2006.04.042

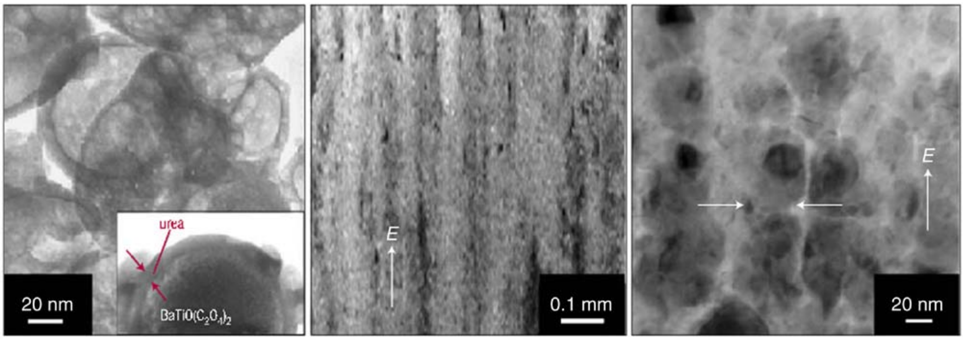

Fig. 1. Images of nanoparticles in GER suspensions. (a) TEM image of coated nanoparticles. Urea coatings are clearly seen. (b) Optical microscopic image of a sample prepared in epoxy, solidified under an applied field E of 2 kV/mm. Columns aligned along the field direction are visible. (c) TEM image of a section of the column shown in (b). The arrows indicate one of the flattened interfaces.

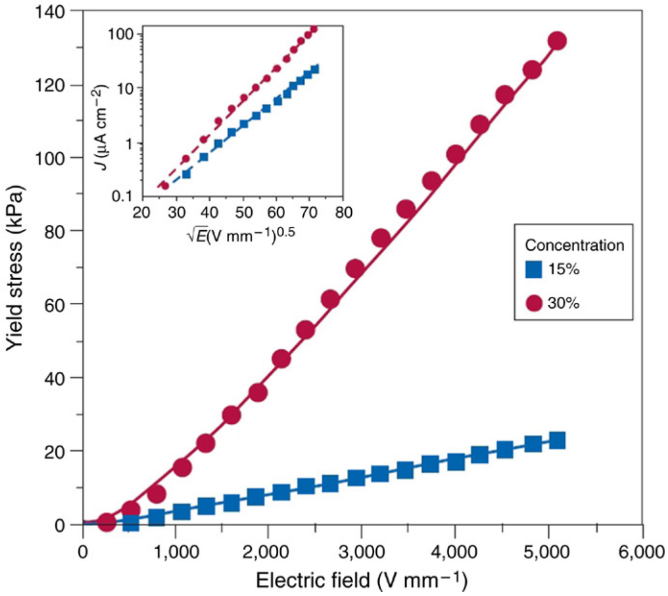

Fig. 2. Static yield stress plotted as a function of applied electric field for two solid concentrations. Symbols denote experiment; solid lines are theory. Inset: logarithm of the current density J plotted as a function of $\sqrt{E}$. The dashed straight lines serve to delineate the relationship $\ln J \propto \sqrt{E}$, indicating the mechanism of activation over the Coulomb barrier.

the sample with solid particle volume fraction of ∼30% (with a zero-field viscosity of 100 Poise), the yield stress can reach 17 kPa at $E = 1$ kV/mm and increases to 130 kPa at 5 kV/mm.

The corresponding current densities are shown in the inset. The current density J is below 4 μA/cm^2 for $E < 2$ kV/mm, and increases to 110 μA/cm^2 at 5 kV/mm for the 30% sample. It has a wide operational temperature range of 10–120 °C; the working current density is low and the reversible response time is less than 10 ms.

Two distinct features of the GER fluids are noted in Fig. 2. To describe the basis of comparison, we first make a brief digression on the "conventional ER fluid mechanism", based on induced polarization (owing to the dielectric constant contrast between the solid particles and the fluid) of suspended dielectric particles. In the heuristic dipole model for induced particles, a random dispersion is not the lowest energy state. Instead, the polarized particles would tend to form chains, and the chains would coalesce into columns at higher field strength. It turns out that an exact treatment of the problem is possible, in which not only the dipole interaction but all the higher-order multipoles, local field effect, and electrical conductivity effects were included [13]. In this so-called dielectric ER (DER) model (based on the assumption that components of the ER fluids exhibit linear response to the electric field), theoretical upper bounds on the yield stress may be obtained. It varies as [13]

$$1.38\sqrt{R/\delta} \qquad (1)$$

in units of $\varepsilon_f E^2/8\pi$. Here δ denotes the separation between the surfaces of neighboring particles and ε_f is the dielectric constant of the liquid. For the purpose of calculating the magnitude of the upper bound, it is generally taken to be 1–2 Å. Several aspects of this expression should be noted. First, the yield stress varies as the square of the applied electric field. This follows from the fact that the yield stress is proportional to the electrostatic energy density $-\mathbf{P}\cdot\mathbf{E}$, where $\mathbf{P}$ is the polarization density. If the polarization is induced, then in the linear regime $\mathbf{P}$ is proportional to $\mathbf{E}$; hence the square dependence on $\mathbf{E}$. Second, the upper bound scales as the square root of particle size. In other words, the induced polarization mechanism favors larger particles. This behavior has been experimentally verified [19]. Third, for a fixed electric field and particle size, there is a maximum value for the yield stress, given by Eq. (1). We shall see that the GER effect violates all three aspects of the induced polarization DER model. Hence it represents a new paradigm that requires new modeling considerations.

From Fig. 2, it is seen that the yield stress can be over 100 kPa. For a particle size of 50–80 nm, this value is more than one order of magnitude larger than the upper bound. The electric field variation is seen to be mostly linear instead of quadratic, indicating a constant (saturated) polarization. As we will see later, the particle size scaling behavior is also opposite to that predicted by Eq. (1). The purpose of this article is to give an explanation of the GER effect. In what follows, we first present the model of aligned dipolar layers in Section 2, and show that it can yield predictions, detailed in Section 3, in excellent agreement with the experiments. In Section 4 the statistical mechanical underpinnings of the model are examined through Monte Carlo simulations. We propose electrowetting, with hydrogen bonding as an contributing element, in inducing the alignment layers by energetically favoring the aligned state in the form of lower interfacial energy between the particles and the suspending liquid.

2. Saturation polarization model

The solid particle of the GER fluids consists of a core of amorphous, porous $BaTiO(C_2O_4)_2$, coated with a liquid-like layer of urea. An important observation about the GER colloid is its large dielectric constant (measured by an LCR meter (HP 4192)), on the order of 50–60 over the temperature range 10–120 °C for the dense samples (>30% solid volume fraction). Since silicone oil has a dielectric constant of ~ 2, this large value is attributed to the coated nanoparticles, where the focus is on the coating. However, the dielectric constant of bulk urea is relatively small, about 3.5, although urea is known to have a large molecular dipole moment of $\mu \approx 4.6$ Debye (and a molecular number of 1.3×10^{22} cm^{-3}). Thus urea, in the form of thin coatings, has a significantly larger dielectric response due to the existence of the interfaces. In particular, the short-range (non-dipolar) interaction between the coating molecules and the core (barium titanium oxalate) particle, and/or the interaction of the molecular dipoles on the oil-coating interfaces, must be such that the molecular dipoles in the coating are not locked into anti-parallel pairs, which would mean insensitivity to the external field and hence a small dielectric response. This is supported by an estimate of the polarizability α based on the free-dipole model, $\alpha = \mu^2/3k_BT$, where k_B is the Boltzmann constant and T the temperature (=300 K), which yields a dielectric susceptibility $\chi \approx 5$ (with a molecular volume of ≈ 100 Å^3), implying a dielectric constant $\varepsilon = 1 + 4\pi\chi \approx 60$ that is in reasonable agreement with the measured value. It is envisioned that there is water inside the porous core (almost inevitable from the fabrication process), and the presence of water plays a role in the formation of the urea coating layer and its liquid-like state.

We propose the mechanism of saturation surface polarization, in the elastic contact region of the neighboring spheres, to be responsible for the observed GER effect. In Fig. 3 we show a schematic picture of our model, consisting of two spherical coated particles whose centers are aligned along the direction of external electric field, with a (flat) deformed contact area. The parameters of the model are stated in the caption.

The contact region is modeled by a 5–10 Å gap separating the flattened surfaces of the two spheres, with the size of the contact region determined by the Hertzian solution [20] of two elastic spheres in contact, pushed together by a force **F**. The final results of our model are insensitive to the exact separation of the gap region, to be shown later. The crucial element of our model is that in the contact region the surface dipoles form two aligned layers, as shown in the right panel of Fig. 3, in contrast to other surface areas where such a (saturation) polarization configuration represents a higher energy state. The aligned dipole layers give rise to an electrostatic force **F** holding the two particles together. Hence the equilibrium contact state is represented by the balance of the electrostatic force with the elastic force. Perturbation from the equilibrium state can be in the form of either shearing in the direction perpendicular to the electric field, or pulling (or compression) along the electric field direction. The shear stress or extensional stress at which the two spheres irreversibly lose contact is denoted the yield stress or tensile stress, respectively. They coincide with the peak in the stress–strain relation (see below), beyond which the stress decreases with increasing strain, indicating instability. Below we first deduce the predictions from this surface polarization model and compare them to the experiments. The statistical mechanics of the aligned surface dipole layers, i.e., the energetics and entropy considerations, will be discussed along with Monte Carlo simulations in Section 4.

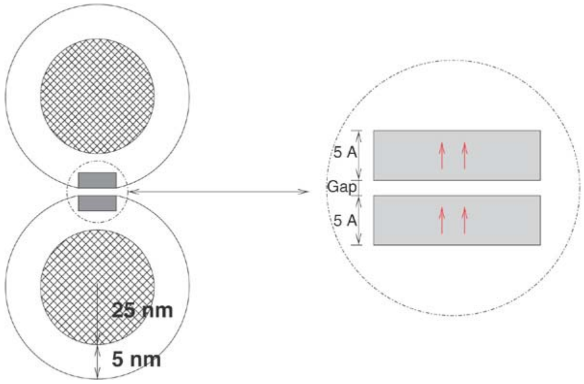

Fig. 3. Surface polarization layer model. The radius of the core is 25 nm and the coating thickness is 5 nm. The gap between two flattened layers is 5–10 Å and the thickness of the saturation polarization layers is 5 Å. The overlap of two spheres is determined by the equilibrium of the electrostatic force and the elastic force.

3. Model predictions

Consider two identical spheres each with radius R (in actual calculations R is taken to be 55 nm, in which 5 nm is the thickness of the coating layer), aligned along the direction of the external electric field. The total energy W consists of two parts: electrostatic and elastic, i.e., $W = W_{\text{es}} + W_{\text{elas}}$. The equilibrium condition is given by $\partial W/\partial h = 0$, i.e., a force balance between the two components, where h is the relative approach of the two spheres. The general expression for electrostatic energy is given by

$$W_{\text{es}} = -\frac{1}{8\pi}\int_{V_o} \mathbf{D}\cdot\mathbf{E}\,\mathrm{d}V - \frac{1}{4\pi}\int_{V_s}\left[\int_0^{\mathbf{E}} \mathbf{D}(\mathbf{E})\cdot\mathrm{d}\mathbf{E}\right]\mathrm{d}V, \tag{2}$$

where V_o is the volume of dielectric materials besides that of the surface (aligned) dipole layer, and V_s is the volume of the surface layer. A separate treatment is needed for the latter due to the nonlinear P–E relation in the surface layers (since the polarization is saturated), which can be roughly approximated by a two-segment function:

$$\mathbf{P} = \begin{cases} \dfrac{|\mathbf{P}_0|}{E_c}\mathbf{E} & \text{if } |\mathbf{E}_{\text{ext}}| \le E_c^{(\text{ext})} \\ \mathbf{P}_0, & \text{if } |\mathbf{E}_{\text{ext}}| > E_c^{(\text{ext})}. \end{cases} \tag{3}$$

Here $\mathbf{E}_{\text{ext}}$ is the externally applied electric field, $E_c^{(\text{ext})}$ denotes the experimental threshold value for saturation polarization and E_c the corresponding microscopic fields inside the layer. The relation is linear when the applied macroscopic electric field is below a threshold value; the polarization $\mathbf{P}$ becomes a constant (saturated) $\mathbf{P}_0$ when the threshold value is exceeded.

Substitution of the two-segment P–E relation into the above equation yields the final energy expression:

$$W_{\text{es}} = -\frac{1}{8\pi}\int_V \mathbf{D}\cdot\mathbf{E}\,\mathrm{d}V - \frac{1}{2}H(|\mathbf{E}_{\text{ext}}| - E_c^{(\text{ext})}) \times \int_{V_s} \mathbf{P}_0\cdot(\mathbf{E}-\mathbf{E}_c)\,\mathrm{d}V, \tag{4}$$

where $V = V_o + V_s$ is the total volume, and $H(x)$ is the step-function which vanishes for $x < 0$, and has value 1 for $x > 0$.

In numerical evaluation of the electrostatic energy, the boundary condition is that there is a voltage difference between two parallel planes (perpendicular to the external electric field) bounding the two spheres. The voltage difference is given by the applied electric field times $4R$. There is an enhancement factor for the local electric field in the contact region, which can be evaluated numerically. By considering only two spheres, our model essentially treats only one chain and neglects the chain–chain interaction.

Calculation of the elastic energy follows that given by the Hertzian solution [20] of two elastic spheres pressed together by a (electrostatic) force $\mathbf{F}$. By using continuum elasticity theory and treating the core as having a negligible effect on the deformation of the coating, one obtains

$$W_{\text{elas}} = h^{5/2}\frac{2}{5D}\sqrt{R/2} \tag{5}$$

where $1/D$ is the deformation modulus, which is the only adjustable parameter in our model. By applying the equilibrium condition (force balance) as stated above, the value of h (and hence the contact area) can be obtained in terms of other given parameters of the problem. The value of the deformation modulus is taken to be that which gives the yield stress (see below) at $E = 2000$ V/mm which is in agreement with the experimental data. Its value is

$$\frac{1}{D} = 0.123\ \text{GPa}. \tag{6}$$

It should be noted that the deformation modulus is comparable to that of liquid, i.e., ~1/10–1/100 those of solids. Once $1/D$ is determined, its value is kept constant in consequent calculations.

For the dispersed nanoparticles with coatings in GER fluids, the elastic properties of the cores may have some effect. As the core is harder than the coating, the contact area between two dispersed particles will be slightly reduced.

3.1. Static yield stress

To calculate the static yield stress, the equilibrium configuration is first calculated under an applied electric field. For $E = 2000$ V/mm, it was found that $h = 1.21$ nm. When the two particles are sheared and thereby tilted, the total energy is dependent on the tilt angle:

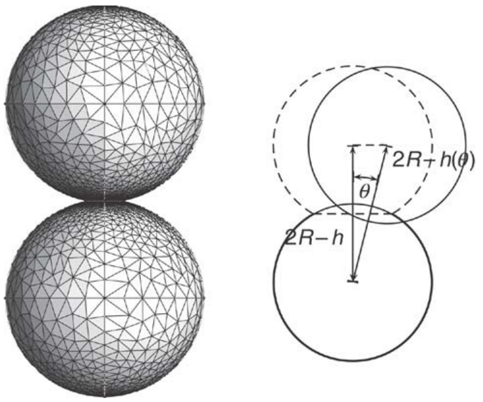

Fig. 4. FEM model for GER fluids. The diameter of the core particle is 50 nm. The thickness of the coating is 5 nm. The dielectric constants of the coating and the core are both taken as 60 and that of silicon oil is 2. A very fine FEM mesh is required in the contact region between the two spheres.

$$W(\theta) = W_{\text{es}}(\theta) + W_{\text{elas}}(\theta). \tag{7}$$

The electrostatic energy can be calculated by direct numerical integration, after solving the electrostatic equation (Laplace equation) by using the finite element method (FEM). The elastic energy can be calculated directly by using the expression

$$W_{\text{elas}}(\theta) = \frac{2}{5D}\sqrt{R/2}[h(\theta)]^{5/2}, \tag{8}$$

where $h(\theta)$ is the difference between $2R$ and the distance of two centers of spheres at angle θ. With the geometric relation shown in Fig. 4, it can be expressed as

$$h(\theta) = 2R - \frac{2R-h}{\cos\theta}. \tag{9}$$

At the detaching point, the angle $\theta_m = \arccos(1-\frac{h}{2R})$, $h(\theta_m) = 0$.

The shear stress is defined as

$$\frac{1}{V}\frac{\partial W(\theta)}{\partial\theta}, \tag{10}$$

and the yield stress is obtained at the detaching angle θ_m when two spheres are separated:

$$Y = \left.\frac{1}{V}\frac{\partial W(\theta)}{\partial\theta}\right|_{\theta=\theta_m}. \tag{11}$$

As seen in Fig. 5, the detachment point also turns out to be the tip of the stress–strain curve, beyond which the system is unstable. Thus by definition the stress at this point is indeed the yield stress.

The static yield stress under different electric field values can be evaluated following the same method as described above, and the results are shown in Fig. 2 as the solid line. Excellent agreement is seen.

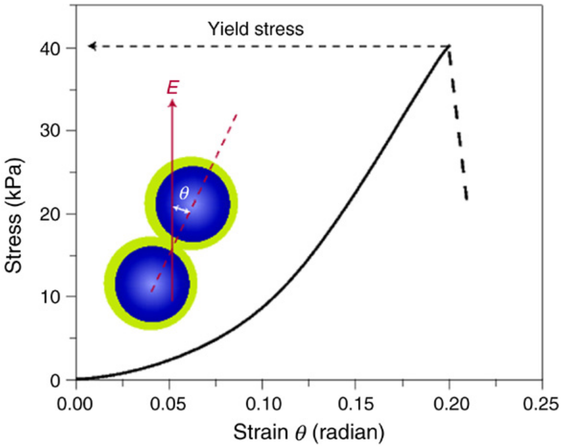

Fig. 5. Calculated static stress–strain (θ) relation at 2 kV/mm. The static yield stress is the peak stress value, beyond which the stress decreases with increasing strain, indicated by the dashed line for instability. There is a discontinuity in the derivative at the yield point. At 2 kV/mm, the equilibrium elastic deformation h is 1.2 nm. The gap width was fixed at 5 Å for all calculations in which the spheres were in elastic contact.

3.2. *Young modulus and tensile stress*

To evaluate the Young modulus and tensile stress, we first determine the equilibrium point at $E = 1000$ V/mm, which is found to occur at $h_0 = 0.74$ nm. The stress F/A is thus given by

$$\frac{F}{A} = -\frac{1}{A}\frac{\partial W}{\partial h}, \tag{12}$$

in which we take $A = (2R)^2 = 3600$ nm^2. The above stress–strain relation is plotted in Fig. 6. At $h = h_0$, the stress F/A is noted to vanish as shown. Expansion of F/A around $h = h_0$ yields

$$\frac{F}{A} = -\frac{1}{A}\frac{\partial W}{\partial h} = -\frac{1}{A}\left[\left.\frac{\partial^2 W}{\partial h^2}\right|_{h=h_0}(h-h_0) + \cdots\right]. \tag{13}$$

In the linear range, the Young modulus is obtained as

$$Y = \frac{L}{A}\left.\frac{\partial^2 W}{\partial h^2}\right|_{h=h_0} = \frac{1}{V}\left.\frac{\partial^2 W}{\partial (h/L)^2}\right|_{h=h_0}, \tag{14}$$

where $L = 2R$. We obtain

$$Y = \frac{L^2}{V}\frac{3}{2D}\sqrt{R/2}\,h_0^{1/2} = 10.3 \text{ MPa} \tag{15}$$

at 1000 V/mm of applied field. Here the volume is taken to be $V = (2R)^3$ in the calculation of the overall energy density.

The tensile stress is the stress at which two spheres become detached, i.e., at $h = 0$. Our evaluation shows that

$$Y_t = 85.3 \text{ kPa} \tag{16}$$

at 1000 V/mm. It is noted that the tensile strength is much larger than the yield stress under the same applied field (∼17 kPa).

Young modulus and tensile stress under different field can be evaluated similarly. The results are plotted in Figs. 7 and 8, respectively.

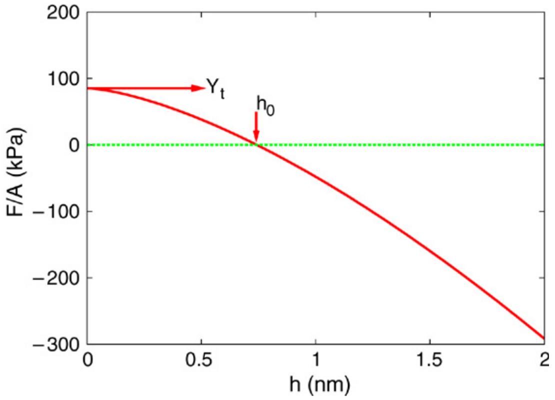

Fig. 6. Calculated stress–strain (h) relation at $E = 1000$ V/mm. The tensile stress is the peak stress value when two spheres are pulled apart, i.e., at $h = 0$.

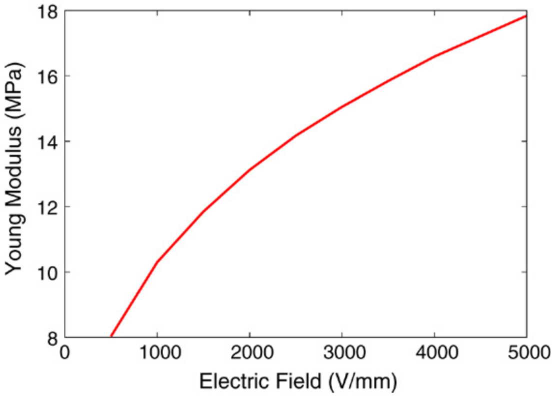

Fig. 7. Field dependence of Young modulus in the GER fluid.

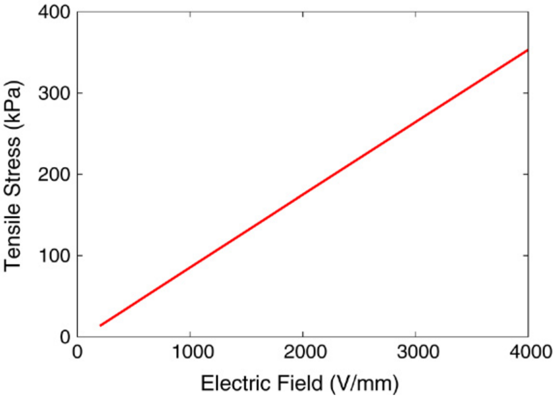

Fig. 8. Field dependence of tensile stress in the GER fluid.

3.3. *Size scaling of the GER effect*

The size dependence of ER fluids is seldom addressed in literature. In the conventional ER mechanism of linear induced polarization, the ER effect increases with the size of the particles as noted before [13]. However, the opposite trend was observed in a recent experiment on GER fluids. Fig. 9 shows a comparison of the measured yield stress for two samples consisting of two different particle sizes. It is observed that the

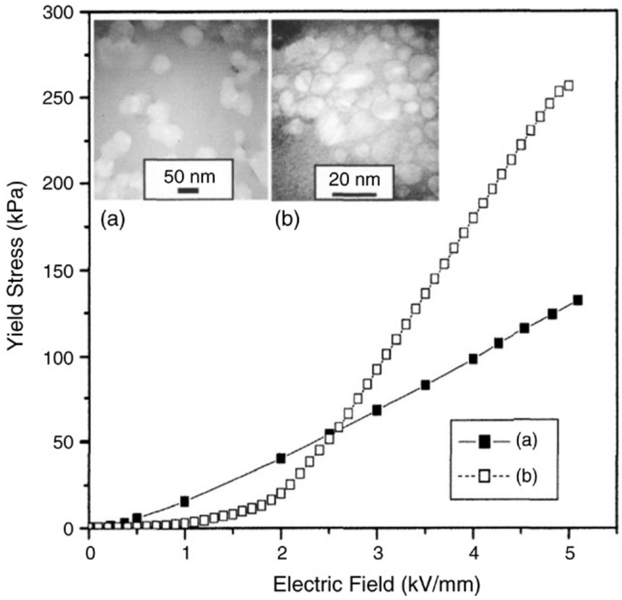

Fig. 9. TEM images of coated nanoparticles. In (a) the nanoparticles were fabricated without Rb addition, and in (b) the nanoparticles were fabricated with Rb addition to the core materials. A clear difference in size is seen, where the size of the particles in inset (a) is almost twice that in inset (b).

(Rb-doped) GER fluids exhibit very strong yield stress — up to 250 kPa at 5 kV/mm. Thus particles about 1/2 the size led to a doubling of the maximum attainable yield stress.

The size scaling behavior of the GER effect can be understood on the basis of the proposed surface polarization model, in which the ER effect originates from the two saturated polarization layers at the contact region of two coated nanoparticles. As the contact region may be regarded as a tiny parallel-plate capacitor, its energy is approximately given by $\mathcal{E}wA$, where $\mathcal{E}$ denotes the (roughly constant) average energy density inside the contact region, w the gap width, and A the contact area. From numerical simulations, it is found that $A \propto R^2$, where R is the radius of the coated particles. Hence if we ignore the much smaller energy elsewhere, then the overall energy density is proportional to $1/R$. This is in reasonable accord with the observed correlation between the yield stress, proportional to the overall energy density, and the particle size.

3.4. Electrical current density

Under high electric field, especially the high local field in the contact region, the molecular dipoles of urea can thermally dissociate due to the reduced Coulomb energy barrier (from the counter-ion), giving rise to free ions and hence charge carriers that are responsible for the electrical current density observed in GER fluids. To model the dissociation process, consider an ion with charge q attracted to the counter-ion by Coulomb potential

$$V_1(r) = -\frac{q}{r}, \tag{17}$$

where r is the radial distance to the counter-ion. When an electric field E is applied along the dipole direction, an additional potential $-Er$ is added, so the total potential is given by

$$V_2(r) = -\frac{q}{r} - Er. \tag{18}$$

It is straightforward to show that the barrier is lowered by an amount

$$\Delta V = -2\sqrt{qE} \tag{19}$$

due to the application of the electric field. This is the well-known Poole–Frenkel effect [21]. The electric-field dependent part of the thermal dissociation probability is given by $\exp[-\Delta V/k_B T]$, where k_B is the Boltzmann factor and T denotes temperature. The current density is obtained by Ohm's law:

$$\mathbf{J} = \sigma \mathbf{E}. \tag{20}$$

Here the conductivity $\sigma = nq\mu$; q is the charge of carriers and μ the mobility. The density of carriers, n, is the fastest varying parameter in this case. Therefore the electric-field dependent part of the carrier density varies as

$$n \propto \exp\left(-\frac{\Delta V}{k_B T}\right), \tag{21}$$

or

$$\ln J \propto \ln n \propto -\Delta V \propto \sqrt{E}. \tag{22}$$

This behavior is indeed confirmed experimentally (shown in the inset of Fig. 2).

3.5. Model parameter considerations

In the induced polarization model, the yield stress increases with the ratio between the particle and fluid dielectric constants. In particular, a theoretical upper bound [13] is obtained in the limit $|\varepsilon/\varepsilon_f| \to \infty$.

Is there also a dielectric constant-dependent effect for the GER fluids? Physically, the induced attractive electrostatic forces between nanoparticles would increase with increased effective dielectric constant of the coated particles, so the neighboring spheres will press upon each other with a stronger force and thereby increase the contact area, leading to enhanced yield stress. The numerical results are shown in Fig. 10, in which the dielectric constant of the particles (core and coating assumed to have the same dielectric constant) is varied from 10 to 2000 and the dielectric constant of the fluid is kept constant as 2. The trend shows an upper limit for the static yield stress when the dielectric constant of the nanoparticles increases.

In another parameter consideration, the gap between two aligned dipolar layers was slightly varied from 5 to 10 Å, distances on the order of atomic separations. The numerical results are shown in Fig. 11. It is seen that the static yield stress is not very sensitive to the gap width between the two layers. This behavior can be understood as follows. If the gap region is considered to be a tiny parallel-plate capacitor, then the electric field in the gap should be almost uniform (since the surface charge density is a constant). Hence the interaction between the two plates is constant, provided that the gap is smaller than the

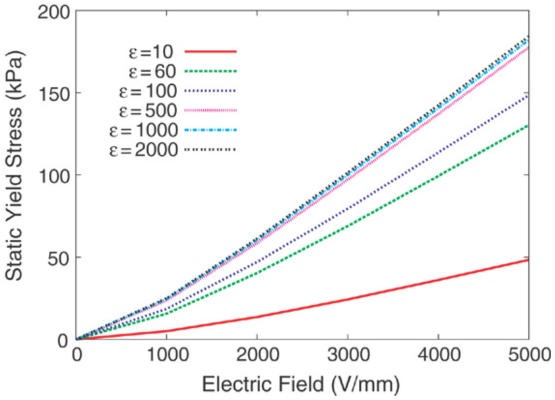

Fig. 10. Dielectric constant mismatch in GER fluids. In a coated particle with a 50 nm diameter core and a 5 nm coating, the dielectric constants of the core and the coating are taken as the same value, varying from 10 to 2000 (shown by different curves). The 5 Å gap has $\varepsilon_f = 2$.

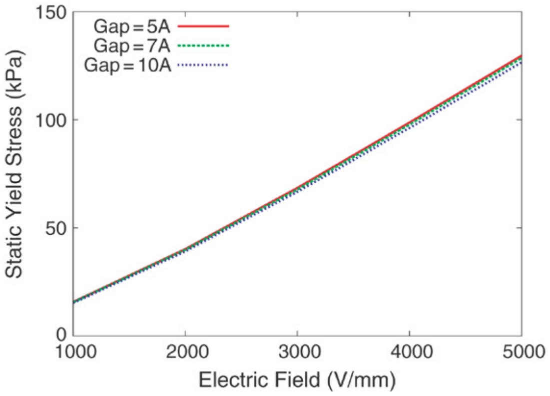

Fig. 11. Static yield stress with different gap width between two saturation layers.

size of the plates. This condition holds in our case, since the gap varies from 5 to 10 Å while the radius of the contact area is about 6 nm when $E = 2$ kV/mm. When the gap separation is comparable to the size of the contact area, a noticeable variation of yield stress is expected.

4. Statistical mechanics of surface aligned layers

In order to investigate the formation of the surface dipolar layers from the statistical mechanic point of view, the contact area of the urea coating are modeled by two cubic lattices ($8 \times 8 \times 8$ each). A urea molecule is put on each lattice site and is simplified as a dipole with a permanent moment (4.6 Debye), the same as that for bulk urea. The dipoles in the outermost layer, i.e., at the coating–core interface, are fixed in anti-parallel pairs, simulating the locked state in bulk urea. The dipoles in other layers can rotate freely as in the liquid state and the dipole–dipole interaction energy is given by

$$W_{ij} = \frac{\mathbf{p}_i \mathbf{p}_j}{r_{ij}^3} - \frac{3(\mathbf{p}_i \cdot \mathbf{r}_{ij})(\mathbf{p}_j \cdot \mathbf{r}_{ij})}{r_{ij}^5}. \tag{23}$$

At the innermost layers, corresponding to the coating–oil interfaces, an additional "electrowetting" effect is proposed which gives rise to perpendicularly-aligned dipoles on the same layer. This is detailed below.

It has been observed in experiments that particle–oil wetting plays a crucial role in the GER effect. Non-wetting can imply no GER effect. Thus a synergistic effect between the particles and the suspending oil exists and is responsible for the appearance of the GER effect. We propose that the electrowetting effect plays a role in the energetics of the aligned dipole layers, by lowering the energy of the aligned dipoles as compared to the usual anti-parallel alignment in the locked configuration (in bulk urea, for example). It is known that the electrowetting effect may be expressed by the Lippmann equation [22,23]:

$$\gamma = \gamma_0 - cE^2, \tag{24}$$

where γ is the surface tension and E is the magnitude of the local electric field. c is a small length scale measured in Å's. The electro-wetting effect is generally small when the local electric field is weak. However, if the dipoles are aligned, the local field can be enormous (on the order of 10^7 V/cm), leading to a significant lowering of the surface energy. This electrowetting effect would mean that (1) the dipoles are not only favored to be aligned, but also to be perpendicular to the layer, as otherwise the electric field would be weak in the fluid region; (2) the effect remains the same if the dipoles are reversed in their orientations; and (3) the effect would counter the repulsive intra-layer interaction between parallel-aligned dipoles in the same layer, acting in conjunction with the attractive inter-layer interaction across the gap.

In mean-field form, the electrowetting effect may be expressed as

$$W_i = -J \sum_j p_i^z p_{j \neq i}^z. \tag{25}$$

Here the superscript on p denotes the component of the dipole perpendicular to the layer, and J is a positive parameter whose microscopic origin will be explored below. Here we first consider the necessary magnitude of J to realize the aligned dipolar layers.

In order to account not only the energetics but also the entropy effects, we have carried out Monte Carlo simulations on the model. It was found that if J is assumed to be 0.4 eV, with the lattice constant being the same as that in bulk urea, i.e., $a = 5$ Å and the gap between two innermost layers being 5 Å, and at the room temperature and under a local electric field 7×10^6 V/cm, the surface aligned dipole layers can be stabilized, as seen in Fig. 12. For a weaker electrowetting effect, i.e., $J < 0.4$ eV, the aligned dipole layers are not stable. Here $J = 0.4$ eV corresponds to a value of $c = 16$ Å in Eq. (24), obtained by the difference of surface energy densities on the contact layers (with and without the electric field), divided by the square of local electric field (the threshold value $E_c = 0.7 \times 10^7$ V/cm, obtained numerically from an $E_c^{(\text{ext})} = 500$ V/mm).

There can be two elements contributing to the electrowetting effect. The first element is the hydrogen bonding interaction. An illustration of the plausible hydrogen bonding network is

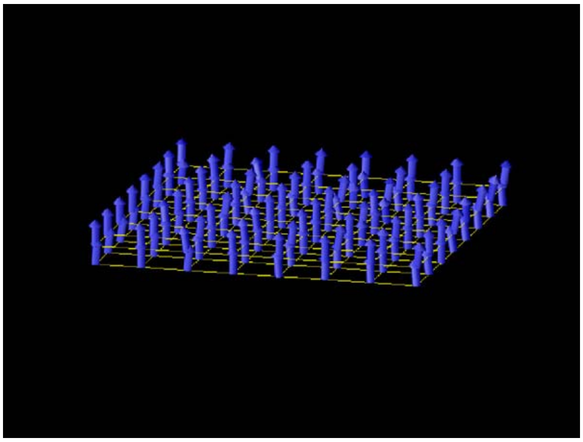

Fig. 12. Monte Carlo simulation result shows the aligned dipolar layers. Here we show mostly the inner layers in the gap region, i.e., the 8th and 9th layers.

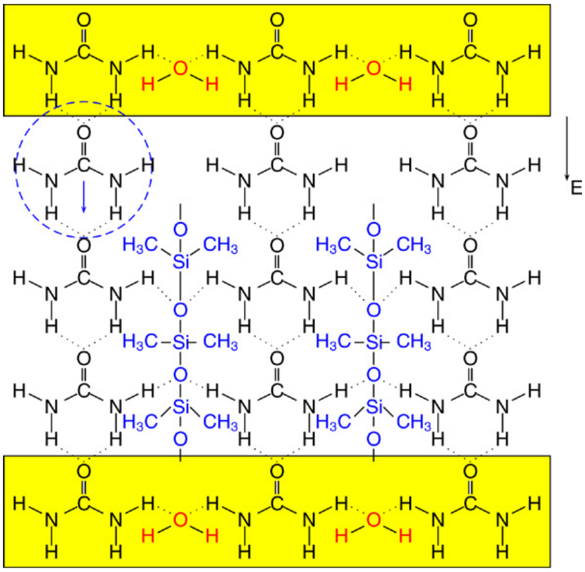

Fig. 13. A schematic hydrogen bonding (indicated by the dotted lines) network favoring the formation of parallel alignment of urea molecular dipoles. The urea molecular dipole unit is indicated by the dashed line, with direction as shown.

shown in Fig. 13, where it is assumed that in the gap region there can be some urea molecules, some water molecules, plus the silicone oil molecules. They network together to give rise to the favorable effect of parallel alignment of the urea molecular dipoles. As each hydrogen bond is on the order of 0.1 eV, it can be seen that the proposed network can contribute a considerable amount to the required $J = 0.4$ eV. The second element is the $-\alpha E^2$ interaction energy between the induced polarization of the molecules in the gap (α being the polarizability) and the local electric field. That energy can also be on the same order, provided the local electric field is on the order of 10^7 V/cm. It is seen that the silicone oil, with the presence of oxygen in its structure, can partly contribute to the hydrogen bonding network. It is conjectured that the presence of oxygen in silicone oil is a contributing factor to its synergistic wetting of the coated nanoparticles.

5. Concluding remarks

We have proposed a surface polarization saturation model for the GER effect, with predictions in excellent agreement with the experiments. The statistical mechanical underpinnings of the aligned dipolar layers were studied by using Monte Carlo simulations, with elements of hydrogen bonding contributing to the energetics favorable to the formation of such layers. Shortcomings of the present approach include the neglect of inter-chain interactions (as the model considers only two particles in a single chain), as well as the lack of a more ab initio justification for the hydrogen bonding model. These constitute tasks to be further pursued.

Acknowledgement

We wish to acknowledge the support of grants from Hong Kong RGC (No. 604104).

References

[1] H. Block, J.P. Kelly, Journal of Physics D: Applied Physics 21 (1988) 1661.

[2] A.P. Gast, C.F. Zukoski, Advances in Colloid and Interface Science 30 (1989) 153.

[3] T.C. Jordan, M. Shaw, IEEE Transactions on Electrical Insulation 24 (1989) 849.

[4] C.F. Zukoski, Annual Review of Materials Science 23 (1993) 45.

[5] K.D. Weiss, J.D. Carlson, J.P. Coulter, Journal of Intelligent Material Systems and Structures 4 (1993) 13.

[6] M. Parthasarathya, D.J. Klingenberg, Materials Science and Engineering: R: Reports 17 (1996) 57.

[7] T.C. Halsey, W. Toor, Physical Review Letters 65 (1990) 2820.

[8] R. Tao, J.M. Sun, Physical Review Letters 67 (1991) 398.

[9] H.J.H. Clercx, G. Bossis, Physical Review E 48 (1993) 2721.

[10] R.A. Anderson, in: R. Tao (Ed.), Proceedings of the International Conference on Electrorheological Fluids: Mechanisms, Properties, Structure, Technology and Applications, World Scientific, Singapore, 1992, pp. 81–90.

[11] N. Felici, J.N. Foulc, P. Atten, in: R. Tao, G.D. Roy (Eds.), Proceedings of the International Conference on Electrorheological Fluids: Mechanisms, Properties, Technology and Applications, World Scientific, Singapore, 1994, pp. 139–152.

[12] L.C. Davis, J.M. Ginder, in: K.O. Havelka, F.E. Filisko (Eds.), Proceedings of an American Chemical Society Symposium on Electrorheological (ER) Materials and Fluids: Progress in Electrorheology: Science and Technology of Electrorheological Materials, Plenum Press, New York, 1995, pp. 107–114.

[13] H.R. Ma, W.J. Wen, W.Y. Tam, P. Sheng, Advances in Physics 52 (2003) 343.

[14] K.P. Tan, R. Stanway, W.A. Bullough, Mechanics of Advanced Materials and Structures 13 (2006) 1.

[15] T. Nakamura, N. Saga, IEEE/ASME Transaction on Mechatronics 10 (2005) 154.

[16] L. Liu et al., Applied Physics Letters 87 (2005) 104106.

[17] N.M. Wereley, J. Lindler, N. Rosenfeld, Y. Choi, Smart Materials and Structures 13 (2004) 743.

[18] W.J. Wen et al., Nature Materials 2 (2003) 727.

[19] W.Y. Tam et al., Physical Review Letters 78 (1997) 2987.

[20] L.D. Landau, E.M. Lifshitz, Theory of Elasticity, 3rd ed., Pergamon Press, Oxford, England, 1986.

[21] J. Frenkel, Physical Review 54 (1938) 647.

[22] G. Lippmann, Annals of Physics 149 (1873) 546.

[23] G. Beni, S. Hackwood, Applied Physics Letters 38 (1981) 207.